

Measurements of Thermophysical Properties of Nickel with a New Highly Sensitive Pyrometer¹

W. Obendrauf,² E. Kaschnitz,² G. Pottlacher,² and H. Jäger²

A new, sensitive, and fast (response time, 100 ns) pyrometer used for the measurement of temperature in pulse heating experiments is described. The monochromatic instrument may use two detectors, namely, a Si diode and an InGaAs diode. Since monochromatic pyrometers usually are "self-calibrated" with the plateau of the melting transition of the investigated metal, a high sensitivity is desirable. The pyrometer is sensitive down to 1000 K and may be used at the melting plateau of copper, a reference point on the International Temperature Scale of 1990. A wide temperature range in a single measurement is possible with the use of a fast operational amplifier with linear and logarithmic outputs. Electrical resistivity, heat capacity, and enthalpy of nickel were measured in the temperature range 1500 to 2200 K using a fast pulse heating technique.

KEY WORDS: electrical resistivity; enthalpy; heat capacity; high-speed pyrometry; high temperatures; liquid metals; nickel; pulse heating.

1. INTRODUCTION

Temperature is an important quantity to be measured when investigating thermophysical properties of metals using pulse heating techniques. Recently a new discharge apparatus, which allows more accurate measurements of current and voltage, was developed in our laboratory [1]. The aim of the work related to the present paper was to improve the determination of temperature, which is based on measuring the spectral radiance of the

¹ Paper presented at the Third Workshop on Subsecond Thermophysics, September 17–18, 1992, Graz, Austria.

² Institut für Experimentalphysik, Technische Universität Graz, Petersgasse 16, A-8010 Graz, Austria.

wire surface. Based on Planck's law, the following relation gives radiance intensity J at temperature T :

$$J(T) = g \int_{\lambda=0}^{\infty} \sigma(\lambda) \tau(\lambda) \varepsilon(\lambda, T) \frac{c_1}{\lambda^5 [\exp(c_2/\lambda T) - 1]} d\lambda \quad (1)$$

where g is a geometric factor, λ is the wavelength, σ is the spectral sensitivity of the detector, τ is the transmittance of the optical systems, ε is the normal spectral emissivity, and c_1 and c_2 are the first and second radiation constants, respectively.

The main problem in surface temperature measurements using pyrometry is due to the necessity of knowing the spectral emissivity $\varepsilon(\lambda, T)$, which is often unknown for liquid metals. Two schools of thought seem to exist on the best approach to minimize the problem: some investigators try to keep the uncertainty of the determination of temperature small using measurements at many wavelengths, whereas others recommend confining the measurements to only one wavelength. Multiwavelength pyrometry tries to determine both temperature and emissivity, by measuring the spectral radiance of the surface at different wavelengths. Therefore, a mathematical model for the dependence of emissivity on wavelength must be assumed. The validity of the assumption cannot be determined from the experimental data, and the magnitude of the resulting systematic error cannot be predicted [2]. Multiwavelength pyrometers have been developed and described by various investigators [3–5].

The pyrometer in the present paper uses only one wavelength, selected by narrow-band interference filters (either at 850 nm, bandwidth 20 nm, or at 1500 nm, bandwidth 40 nm) to detect surface radiation intensity with either Si or InGaAs photodiodes. Temperatures are calculated using Planck's law and forming ratios of the radiance at temperature T to the radiance at the known melting temperature T_M .

At melting (index M) the pyrometer detects a constant radiance with intensity J_M at only one wavelength,

$$J_M(T_M) = g\sigma(\lambda) \tau(\lambda) \varepsilon(\lambda, T_M) \frac{c_1}{\lambda^5 [\exp(c_2/\lambda T_M) - 1]} \quad (2)$$

where $J_M(T_M)$ is the measured radiance intensity at the melting point, and T_M is the melting temperature. At any point in the liquid phase the pyrometer detects a radiance intensity, $J(T)$

$$J(T) = g\sigma(\lambda) \tau(\lambda) \varepsilon(\lambda, T) \frac{c_1}{\lambda^5 [\exp(c_2/\lambda T) - 1]} \quad (3)$$

where $J(T)$ is the measured radiance intensity at temperature T . The unknown temperature T is obtained from the ratio

$$\frac{J_M(T_M)}{J(T)} \quad (4)$$

using Eqs. (2) and (3), leading to

$$T = c_2 / \lambda \ln \left\{ 1 + \frac{J_M(T_M) \varepsilon(\lambda, T)}{J(T) \varepsilon(\lambda, T_M)} \left[\exp \left(\frac{c_2}{\lambda T_M} \right) - 1 \right] \right\} \quad (5)$$

Since the emissivity of most liquid metals is unknown, an assumption has to be made for the ratio $\varepsilon(\lambda, T)/\varepsilon(\lambda, T_M)$ in Eq. (5). Generally a constant emissivity is assumed for the liquid phase (i.e., Refs. 6–9), and consequently our results are based on the assumption that $\varepsilon(\lambda, T)/\varepsilon(\lambda, T_M) = 1$.

If the melting plateau for materials under study cannot be resolved, other calibration points, in general well-reproducible melting transitions of metals with high melting points, have to be used [10]. In this case, the uncertainty of temperature measurement increases due to the following reasons.

- (a) It is no longer possible to assume $\varepsilon(\lambda, T)/\varepsilon(\lambda, T_M) = 1$, but at the melting point the emissivity of the specimen as well as the emissivity of the metal used for calibration has to be known. This does not often occur.
- (b) The geometric factor g can change, because two different experiments for measurement and calibration are necessary. Then geometric factors do not cancel in the deviation of Eq. (5).

2. THE NEW PYROMETER

2.1. Optical Design

Figure 1 shows the optical part of the pyrometer. The optical fiber is randomly bundled and has a rectangular entrance (9.8×0.7 mm) at one side. A lens (2) produces an image of the sample (1) at the entrance of the optical fiber. Figure 2 presents the image of the wire at the rectangular entrance (11) of the optical fiber. The entrance is also used as an aperture stop.

The mirror (4) in Fig. 1 is used to control the adjustment of the image of the wire with a viewing telescope. The rectangular end of the optical fiber is fixed in a holder, which can be turned, and can be adjusted horizontally as well as vertically.

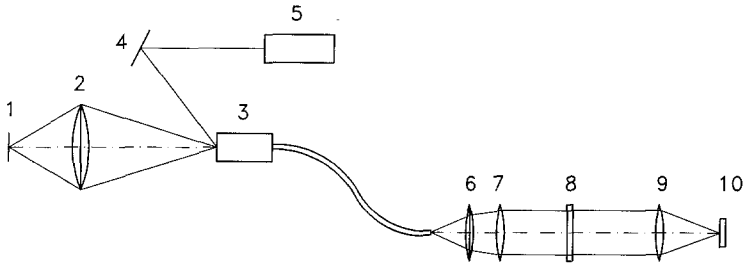


Fig. 1. Optical part of the pyrometer: 1, wire sample; 2, lens ($f = 70$ mm); 3, light fiber with rectangular entrance; 4, mirror; 5, telescope; 6, lens ($f = 12.5$ mm); 7, lens ($f = 25$ mm); 8, interference filter; 9, lens ($f = 30$ mm); 10, PIN photodiode (Si or InGaAs).

The optical parts of the pyrometer that have been described so far are mounted on an optical bench. The other parts are shielded in a metal box (to prevent interference from the electrical discharge) together with the photodiode used as detector and the amplifiers.

As Fig. 1 shows, the light that emerges from the circular end of the fiber is collimated with the help of lenses (6 and 7) and focused on a photodiode (10) after passing through an interference filter (8). For adjustment, all optical parts located in the casing can be moved along the optical axis.

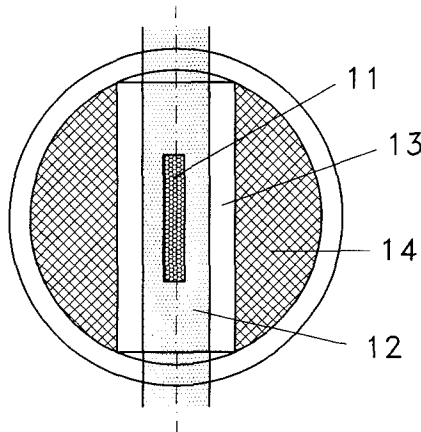


Fig. 2. Image of the wire at the rectangular entrance of the light fiber: 11, entrance of the light fiber; 12, image of the wire sample; 13, light fiber mounting; 14, holder.

2.2. Electronic Design

According to Eq. (1) the intensity of radiation increases exponentially with increasing temperature. A wide dynamic range in a single experiment is obtained by amplifying the detector output simultaneously with linear and logarithmic amplifiers.

Low-noise, fast linear operational amplifiers (AD 846, Analog Devices) are used to transduce the detector current to a signal voltage. Additionally, a fast logarithmic amplifier stage was built (AD 640, Analog Devices). This module is a complete monolithic logarithmic amplifier which is comprised of five cascaded dc coupled amplifier stages.

2.3. Advantages of the New Pyrometer

The main advantages of the new pyrometer are its high sensitivity combined with its short rise time (100 ns) and its wide temperature range covered in a single experiment. Using this pyrometer with an InGaAs detector, we performed measurements at the melting point of copper (given in Ref. 1), one of the reference points on the International Temperature Scale of 1990.

In order to reach a high sensitivity, radiation from a large portion of the wire surface should be received by the diode. Furthermore, it is important that the pyrometer detects only radiation emitted normal to the surface. Both tasks are accomplished by a rectangular light fiber entrance, which is adapted to the form of the wire specimen. The front lens (lens 2 in Fig. 1, focal length $f = 70$ mm), with a diameter $d = 60$ mm, is located near the sample gathering the radiation from the surface. The second lens system located in the shielded metal box is designed to keep the intensity loss as low as possible. Finally, the low-noise operational amplifiers AD 846 lead to a high signal-to-noise ratio.

A further advantage of the pyrometer is the possibility of the simultaneous recording of two signals, taking advantage of linear and logarithmic amplification. The linear amplifier is used to detect the melting temperature region with the melting plateau. The logarithmic amplifier covers a wide signal range. Consequently a wide temperature range is covered in a single experiment and it is no longer necessary to perform several experiments using different field stops in front of the pyrometer in order to adjust for different radiation intensities.

Finally, the projection of the wire by the help of only one lens is easy to adjust and can be controlled with the telescope. No other parts need to be changed or adjusted.

3. THERMOPHYSICAL PROPERTIES OF NICKEL

3.1. Experiments

In investigations on liquid nickel performed earlier [11], the melting plateau was not resolved on radiance intensity traces. Therefore, more accurate measurements were performed with the help of the new sensitive pyrometer. Nickel wire samples (purity, 99.98%; diameter, 0.5 mm; length, 40 mm) from Goodfellows Metals, Cambridge, Great Britain, were used.

Current, voltage, and surface radiance intensity, each as a function of time, were recorded by two digital oscilloscopes. The measuring equipment and the equations used to calculate thermophysical properties are described in another paper [1]. The control of the digital oscilloscopes and collection and evaluation of data were performed by a personal computer.

Figure 3 shows a typical pyrometer signal with a melting plateau on the traces corresponding to the linear as well as the logarithmic amplifier outputs. At temperatures higher than melting, the linear amplifier reaches saturation while the logarithmic amplifier covers the entire range of the experiment. From the radiance data, temperatures can be evaluated according to Eq. (5). Figure 4 shows an example of the calculated temperatures versus time for an experiment.

3.2. Results

By means of least-squares fits, the following polynomials for the relation between enthalpy H and temperature T were obtained from a large number of data points.

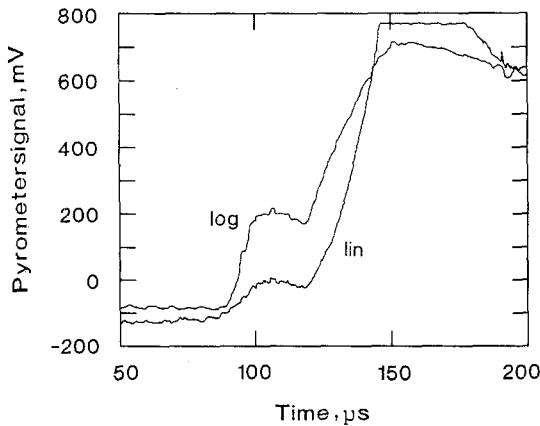


Fig. 3. Linear (lin) and logarithmic (log) pyrometer voltage signals as a function of time (t). Nickel wire: length, 38.2 mm; diameter, 0.5 mm. Charging voltage, 6 kV.

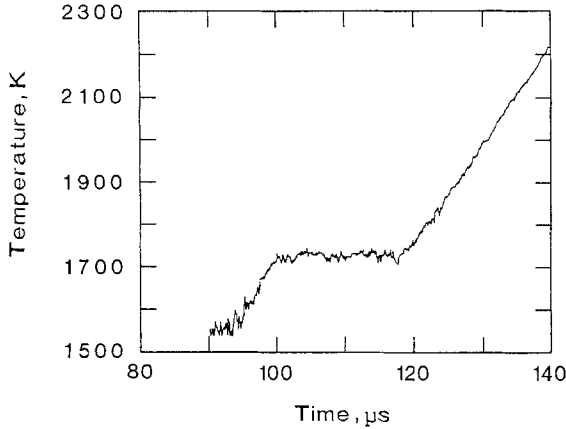


Fig. 4. Temperature versus time. Nickel wire: length, 38.2 mm; diameter, 0.5 mm. Charging voltage, 6 kV.

The best fit in the range of $1500 \text{ K} < T < T_M$ is given by (H in $\text{MJ} \cdot \text{kg}^{-1}$, $T_M = 1728 \text{ K}$, melting point of nickel [19])

$$H = -0.258 + 0.612 \times 10^{-3} T \quad (6)$$

$$T = 422 + 1.63 \times 10^{-3} H \quad (7)$$

and that for the range $T_M < T < 2200 \text{ K}$ by

$$H = -0.207 + 0.760 \times 10^{-3} T \quad (8)$$

$$T = 270 + 1.32 \times 10^{-3} H \quad (9)$$

The enthalpy as a function of temperature for nickel is plotted in Fig. 5. Enthalpy at the beginning (H_S) and at the end (H_1) of the melting plateau, melting enthalpy ΔH , and specific heat capacity in the solid phase [$c_p(S)$] and in the liquid phase [$c_p(L)$] are listed in Table I.

The best fit to our data for electrical resistivity ρ_0 (without correction for thermal expansion) as a function of temperature T for the range $1500 \text{ K} < T < T_M$ (ρ_0 in $\mu\Omega \cdot \text{cm}$) is given by

$$\rho_0 = 33.9 + 1.52 \times 10^{-2} T \quad (10)$$

and that for the range $T_M < T < 2200 \text{ K}$ by

$$\rho_0 = 63.0 + 1.26 \times 10^{-2} T \quad (11)$$

The electrical resistivity of nickel (without thermal expansion correction) as a function of temperature is plotted in Fig. 6. The results at the

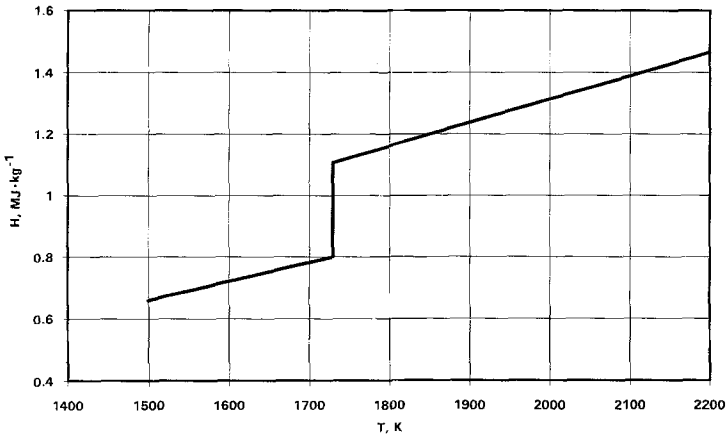


Fig. 5. Enthalpy versus temperature for nickel.

beginning (ρ_{0S}) and at the end (ρ_{0L}) of the melting plateau and the ratio ρ_{0L}/ρ_{0S} are presented in Table II.

Finally, the polynomials (obtained by least-squares fits) for the behavior of electrical resistivity without expansion correction ρ_0 versus enthalpy H are obtained for the range $0.2 \text{ MJ} \cdot \text{kg}^{-1} < H < H_S$,

$$\rho_0 = 19.62 + 71.31 H - 25.47 H^2 \quad (12)$$

and for the range $H_L < H < 1.4 \text{ MJ} \cdot \text{kg}^{-1}$,

$$\rho_0 = 62.85 + 19.64 H \quad (13)$$

Table I. Enthalpy at the Beginning (H_S) and at the End (H_L) of the Melting Transition, Melting Enthalpy ΔH , and Specific Heat Capacity in the Solid Phase [$c_P(S)$] and in the Liquid Phase [$c_P(L)$] of Nickel

Ref. No.	H_S (MJ · kg ⁻¹)	H_L (MJ · kg ⁻¹)	ΔH (MJ · kg ⁻¹)	$c_P(S)$ (J · kg ⁻¹ · K ⁻¹)	$c_P(L)$ (J · kg ⁻¹ · K ⁻¹)
This work	0.800	1.107	0.307	612	760
11	0.802	1.094	0.292		762
14	0.797	1.089	0.292		
12	0.800	1.106	0.306		
13	0.810	1.108	0.298		
15				654	
17					723
18					741

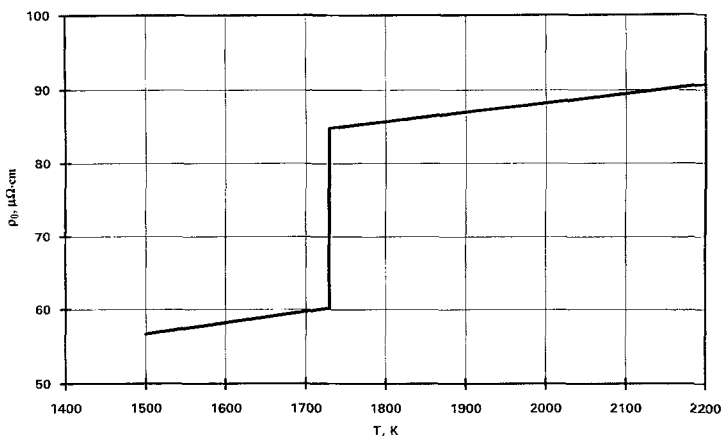


Fig. 6. Electrical resistivity (without thermal expansion correction) versus temperature for nickel.

Results of this work are compared in Tables I and II to the values of other investigators and show, in general, a good agreement.

3.3. Estimation of Errors

An uncertainty of $\pm 3\%$ is estimated for enthalpy and of $\pm 4\%$ for electrical resistivity. Recent measurements [1] with this new pyrometer compare surface radiation to blackbody radiation for a liquid tube. It is shown that the deviation of true temperature in the range 1850 to 2200 K of liquid nickel from that determined with the assumption of a constant spectral emissivity is less than 1.6%, therefore the uncertainty in the temperature measurements on nickel is about $\pm 3\%$ close to the melting

Table II. Electrical Resistivity (not Corrected for Thermal Expansion) at the Beginning (ρ_{0S}) and at the End (ρ_{0L}) of the Melting Transition for Nickel

Ref. No.	ρ_{0L} ($\mu\Omega \cdot \text{cm}$)	ρ_{0S} ($\mu\Omega \cdot \text{cm}$)	ρ_{0L}/ρ_{0S}
This work	60.0	84.7	1.41
11	56.1	76.0	1.35
14	58.9	79.7	1.35
12	67.8	86.3	1.27
16	52.6	80.2	1.52
17	59.5		

transition and should not exceed $\pm 5\%$ for temperatures of 2200 K. The uncertainty in the specific heat capacity therefore should not be more than $\pm 8\%$.

4. CONCLUSIONS

A new pyrometer for pulse heating measurements of thermophysical properties was described. The instrument uses either a Si or an InGaAs detector and is very fast (rise time, 100 ns). It is operated monochromatically with narrow-bandwidth filters either at 850 nm (bandwidth, 20 nm) or at 1500 nm (bandwidth, 40 nm). Using an InGaAs PIN diode as detector, the pyrometer is sensitive down to 1000 K and, thus, capable of measuring the melting plateau of different metals. The instrument was used to measure thermophysical properties of nickel in the temperature range from melting point to 2200 K. The data obtained are in good agreement with those reported in the literature.

REFERENCES

1. E. Kaschnitz, G. Pottlacher, and H. Jäger, *Int. J. Thermophys.* **13**:699 (1992).
2. P. B. Coates, *High Temp. High Press.* **20**:433 (1988).
3. J. L. Gardner and T. P. Jones, *J. Phys.* **13**:306 (1980).
4. J. P. Hiernaut, R. Beukers, W. Heinz, R. Selfslag, M. Hoch, and R. W. Ohse, *High Temp. High Press.* **18**:141 (1986).
5. C. Ronchi, R. Beukers, H. Heinz, J. P. Hiernaut, and R. Selfslag, *Int. J. Thermophys.* **13**:107 (1992).
6. A. Berthault, L. Arles, and J. Matricon, *Int. J. Thermophys.* **7**:181 (1986).
7. G. R. Gathers, *Int. J. Thermophys.* **4**:149 (1983).
8. J. W. Shaner, G. R. Gathers, and W. M. Hodgson, in *Proc. 7th Symp. Thermophys. Prop.*, A. Cezairliyan, ed. (ASME, New York, 1977), p. 896.
9. R. S. Hixson and M. A. Winkler, *Int. J. Thermophys.* **11**:709 (1988).
10. G. Pottlacher and H. Jäger, *Int. J. Thermophys.* **11**:719 (1990).
11. G. Pottlacher, H. Jäger, and T. Neger, *High Temp. High Press.* **19**:19 (1987).
12. U. Seydel, W. Fucke, and H. Wadle, *Die Bestimmung thermophysikalischer Daten flüssiger hochschmelzender Metalle mit schnellen Pulsaufheizexperimenten* (Verlag Dr. Peter Mannhold, Düsseldorf, 1980).
13. R. Hultgren, P. D. Desai, D. T. Hawkins, M. Gleiser, K. K. Kelley, and D. D. Wagman, *Selected Values of Thermodynamic Properties of the Elements* (ASM Metals Park, Ohio, 1973).
14. A. I. Savvatimskii, *Teplofiz. Vysokikh-Temp.* **5**:28 (1990).
15. A. Cezairliyan and A. P. Müller, *Int. J. Thermophys.* **4**:389 (1983).
16. H. J. Güntherodt, E. Hauser, H. U. Künzi, and R. Müller, *Phys. Lett.* **54A**:291 (1975).
17. R. S. Hixson, M. A. Winkler, and M. L. Hodgson, *Phys. Rev. B* **42**:6485 (1990).
18. J. L. Margrave, *High Temp. High Press.* **2**:141 (1968).
19. D. R. Lide (ed.), *Handbook of Chemistry and Physics* (CRC Press, Boca Raton, FL, 1991/1992).